Food Control 119 (2021) 107454

Contents lists available at ScienceDirect

Food Control

journal homepage: www.elsevier.com/locate/foodcont

Detection of chocolate powder adulteration with peanut using near-infrared hyperspectral imaging and Multivariate Curve Resolution

Antoine Laborde [a,b,e,*], Francesc Puig-Castellví [c], Delphine Jouan-Rimbaud Bouveresse [a,b], Luc Eveleigh [c], Christophe Cordella [a,b,f], Benoît Jaillais [d,f]

[a] Groupe "Chimiométrie pour la Caractérisation de Biomarqueurs – C2B", UMR Physiologie de la Nutrition et du Comportement Alimentaire, AgroParisTech, INRAE, Université Paris-Saclay, 75005, Paris, France
[b] Université Paris-Saclay, AgroParisTech, INRAE, UMR PNCA, 75005, Paris, France
[c] AgroParisTech, UMR782 SayFood, INRAE/AgroParisTech/Université Paris-Saclay, Paris, France
[d] Unité de Statistiques, Sensométrie, Chimiométrie INRAE/ONIRIS, Nantes, France
[e] GreenTropism, Paris, France
[f] ChemHouse Research Group, Montpellier, France

ARTICLE INFO

Keywords:
Food safety
Hyperspectral imaging
Near-infrared spectroscopy
Multivariate curve resolution

ABSTRACT

This study aims to detect peanut flour adulteration in chocolate powder using near-infrared (NIR) hyperspectral imaging. Fifteen samples were prepared by mixing both food products in different proportions (0%, 0.1%, 1%, 10% and 100% of peanut) and measured using the hyperspectral camera. A preliminary Principal Component Analysis (PCA) was performed to investigate the structure of the data. Next, the Multivariate Curve Resolution - Alternating Least Squares (MCR-ALS) chemometric method combined with a selectivity constraint in the concentration matrix was applied to untangle the spectral data into a set of components representative of the main constituents found in the samples. Moreover, a detection algorithm based on the calculation of the Mahalanobis distance for every pixel to the model distribution of chocolate powder was implemented. This analysis revealed the complexity of the unmixing problem, allegedly due to the spectral signature overlap in the pixel field of view and because the pure products presented similar spectral signatures. MCR-ALS results were improved after the application of a selectivity constraint, which resulted in a higher performance of the detection algorithm. MCR-ALS detected from 0% to 2.2% of adulterated pixels in mixed samples. On the other hand, the selectivity-constrained MCR-ALS method provided detections from 0.03% to 17.0% in those samples. This pipeline showed that peanut adulteration can be detected even for the lowest concentration level tested (0.1% of peanut). This work highlights the potential of NIR hyperspectral imaging combined with chemometrics for detection purposes.

1. Introduction

In the industry, there is a high interest in detecting contaminations in powders (Fitzpatrick & Ahrné, 2005). Food industry concerns about cross-contamination of ingredients are increasing due to the increasing prevalence of food allergies. On the one hand, for some people, allergic reactions can be triggered with just a few milligrams of pure allergen (Moneret-Vautrin & Kanny, 2004). On the other hand, a significant 4% of the total world population suffers from a form of food allergy (van Hengel, 2007).

Due to the existence of major food allergens such as peanuts (Hefle & Taylor, 2004), food handling in the industry can be especially challenging (Chang, Sreedharan, & Schneider, 2013). In addition, processing methods that focus on powder foods (i.e., producing a dry mix) can increase the risk of food cross-contamination due to the difficulty in cleaning the equipment between two lines of food products in progress (Hefle & Taylor, 2004) and because it is difficult to assess whether all contaminants have been removed after the cleaning phase (van Hengel, 2007). However, several strategies exist to detect product contamination. Most detection strategies consist of direct methods that search for specific target molecules (i.e., proteins, DNA) from the adulterant/contaminant, i.e. allergen, using molecular biology and

* Corresponding author. Groupe "Chimiométrie pour la Caractérisation de Biomarqueurs – C2B", UMR Physiologie de la Nutrition et du Comportement Alimentaire, AgroParisTech, INRAE, Université Paris-Saclay, 75005, Paris, France.
E-mail address: lab.antoine@gmail.com (A. Laborde).

https://doi.org/10.1016/j.foodcont.2020.107454
Received 6 April 2020; Received in revised form 11 June 2020; Accepted 26 June 2020
Available online 7 July 2020
0956-7135/© 2020 Elsevier Ltd. All rights reserved.

immunological methods. For example, the immunological method ELISA detects proteins with a very low sensitivity (from 1 to 2.5 ppm) (Hefle & Taylor, 2004). However, ELISA is a destructive method employed on small sample volumes, which might not be representative enough of the whole sample. Additionally, immunological or molecular biology methods are not optimal for automatic screening because they are expensive and time-consuming.

Alternatively, the rise of the fingerprinting methods has led to the advent of indirect detection strategies. Near-infrared (NIR) spectroscopy method has a particularly high potential for food safety applications (Lohumi, Lee, Lee, & Cho, 2015). NIR enables the fast screening of organic matter, without preparing nor altering the sample. In recent years, hyperspectral imaging has been developed for food safety industrial applications (Gowen, O'Donnell, Cullen, Downey, & Frias, 2007). This technique combines spectroscopy and imaging techniques, enabling the acquisition of hyperspectral images. These images are composed of reflectance pixelmaps containing hundreds of channels, one per wavelength. This measurement technique makes possible to obtain local NIR measurements for each pixel of the hyperspectral image, allowing the observation of the chemical heterogeneity of the samples. Therefore, hyperspectral imaging should be regarded as a promising solution for detecting food contamination in powders.

Some examples of product contamination detection using spectroscopy methods can be found in the literature. For instance, the detection of melamine in milk powder was investigated using line scan NIR hyperspectral imaging (Fernández Pierna et al., 2014) (Fu et al., 2014) (Y. Huang, Tian, Min, Xiong, & Du, 2015) (M. Huang et al., 2016). The detection of crushed peanut in wheat flour was performed by applying Independent Component Analysis (ICA) (Mishra et al., 2016) and Principal Component Analysis (PCA) (Mishra, Herrero-Langreo, Barreiro, & Roger, 2015) to the hyperspectral data. In the pharmaceutical domain, the amount of low dose of magnesium stearate was analyzed using Multivariate Curve Resolution (MCR) and Raman hyperspectral imaging (Boiret, de Juan, Gorretta, Ginot, & Roger, 2015).

Although hyperspectral imaging can provide spectral measurements of a small sample area, the field of view of one pixel is large compared to the particle size of powders. Generally, the pixel size of a NIR hyperspectral imaging system is about 200 μm by 200 μm (Geladi, Burger, & Lestander, 2004) whereas the particle size of some powders, such as flours, may be even smaller than 100 μm (Joint FAO/WHO Codex Alimentarius Commission, 1995). As a consequence, the spectral profile measured in a pixel is not representative of one particle but of several ones. Thus, if these particles correspond to different chemicals, the resulting spectrum will be a mixture of the spectral features of the pure chemicals involved. Thus, in the analysis of hyperspectral images for particle detection, the spectrum of each pixel is considered to include a potential mixture of compounds. This is known as the subpixel detecting problem (Bioucas-Dias et al., 2012).

Various chemometric methods (i.e., ICA (Mishra et al. (2016)), MCR (Boiret et al. (2015)), Non-Negative Least Squares (NNLS) (Lancelot, Bertrand, Hanafi, & Jaillais, 2017)) have been used to address this subpixel detecting problem. All these methods showed high-performance results to unmix hyperspectral images, although the data analysis may become challenging when the particles to detect (from the contaminant) have a spectral signature very close to the background particles (belonging to food sample).

When dealing with food contamination, there is no guarantee the spectral features of the contaminant differs from that of the background. For example, this is the case for melamine contamination in milk powder (Fernández Pierna et al., 2014). In the same line, the peanut NIR spectral signature is very similar to cocoa especially when the products are transformed into flour or chocolate powder. These two food compounds are involved in potential allergen contamination cases in the food industry. In agreement with this, a study of the French market showed that 67% of snacking products labels advised of the possible unwanted presence of peanuts in their product (INRA & ANSES, 2015). Thus, assuring the absence of peanut traces in chocolate products is a matter of utmost importance for the food industry.

In this study, we propose to tackle the problem of detecting peanut flour particles in chocolate powder using both the NIR hyperspectral imaging technique and chemometrics methods. First, a PCA was performed as a reference technique and then a detection algorithm based on the MCR-ALS chemometric method was applied. This work provides novel insights into the spectral features of the chocolate-peanut system and presents a methodology to address subpixel detection using hyperspectral imaging with the potential to be implemented in food processing industries. To our knowledge, the study of the detection of food allergens by combining NIR hyperspectral imaging and chemometrics is not common in the literature.

2. Material and methods

2.1. Sample preparation

A chocolate powder mix to prepare milk beverages was purchased in a French supermarket. The main ingredients of the mixture are sucrose, cocoa, dextrose, and soya lecithin. Defatted peanut flour was bought on the German market. The powders were mixed in different mass proportions of peanut flour: 10%, 1%, and 0.1%. For each concentration, three replicate samples of 13 g were prepared. In addition, pure chocolate powder and pure peanut flour samples were also prepared in triplicate, leading to a total of 15 samples. For the spectral measurements, the powders were put in a plastic sample holder made of polylactic acid. The powder was skimmed on the top to achieve a thickness of 7 mm. This thickness ensured that the bottom of the sample holder did not have an influence on the near-infrared reflectance signal measured by the hyperspectral system (Laborde et al., 2019).

2.2. Hyperspectral imaging system

A line-scan pushbroom Specim SWIR camera (Specim, Spectral Imaging Ltd, Oulu, Finland) was used to acquire the hyperspectral images. The system acquires 288 spectral bands from 1000 to 2500 nm with a spectral sampling of 5.6 nm. The spectral range 1000–2500 nm was chosen as it proved its superior capability to analyze the chemical content of peanut compared to the range 400–1000 nm (Jin, Ma, Li, & Cheng, 2016). Additionally, it was successfully used for the measurement of sugar in a similar chocolate powder (da Costa Filho, 2009). The camera was moving along the y-axis and acquired 320 pixels per line to form the hyperspectral cube. Six halogen lamps were used to illuminate the sample. A white diffuse reflectance standard in Teflon was used to acquire the white reference image before each measurement. The dark reference image was acquired by closing the shutter of the camera.

2.3. Data preprocessing

Hyperspectral cubes were cropped in the spatial dimension to obtain the same image size for each sample. Each image was composed of 61 × 61 pixels, which corresponded to a field of view of 1.5 cm × 1.5 cm. The white reference image (I_0) was averaged to obtain one reference spectrum for each pixel of the sensor line. The reflectance cube was calculated using (Eq. (1)) and the dark measurement (I_B).

$$R = \frac{I - I_B}{I_0 - I_B}, \quad (1)$$

Wavelengths from 1000 nm to 1100 nm and from 2400 nm to 2500 nm were removed because they were mainly representative of electronic noise. The remaining spectra were smoothed using a Savitsky-Golay filter (second order polynomial, 7-point window, and with no derivative) and preprocessed with a logarithmic transformation (- $\log_{10}$).

2.4. Hyperspectral cube unfolding

Hyperspectral images can be regarded as tridimensional hyperspectral cubes, where the x and y planes correspond to the spatial dimensions and the z plane contains the hyperspectral data for every pixel (left side in Fig. 1). This cube can be unfolded into a two-dimensional matrix, with as many rows as pixels and as many columns as measured wavelengths (right side in Fig. 1). Every row in this matrix contains the spectrum relative to one pixel. This data unfolding strategy is required to investigate tridimensional data with bilinear methods such as MCR-ALS (Olmos et al., 2017).

2.5. Multivariate Curve Resolution - Alternating Least Squares

Multivariate Curve Resolution-Alternating Least Squares (MCR-ALS) is a chemometric method used to solve the unmixing problem (de Juan, 2020). According to MCR-ALS (de Juan, Jaumot, & Tauler, 2014a), (Tauler & Kowalski, 1993), a matrix **D** containing mixed signal measurements can be decomposed as the product of the pure spectral profiles, **S**, associated with their pure concentration contributions, **C**, using the following bilinear model (Eq. (2)):

$$\mathbf{D} = \mathbf{C}\mathbf{S}^{\mathbf{T}} + \mathbf{E}, \tag{2}$$

where **D** is a n by q matrix containing the spectral data in rows; **C** is a n by k matrix containing the concentration coefficients for each pixel in rows; $\mathbf{S}^{\mathbf{T}}$ is a k by q matrix containing the pure spectral profiles in rows; **E** is a n by q matrix containing the residual information not explained by the model.

In this decomposition, the number of pure profiles to be resolved is determined by the number of components, which needs to be estimated before running the analysis. The number of components can be estimated using the Singular Value Decomposition (SVD) algorithm (Golub & Reinsch, 1970).

MCR-ALS algorithm is an iterative method that optimizes a set of initial estimates for the concentration (**C**) or the spectrum profiles (**S**) under constraints while minimizing the residual part **E**.

In this study, the initial estimates used were the most dissimilar spectra found in the hyperspectral images of the pure samples of peanut flour and chocolate powder. One spectrum was selected for peanut flour, while two spectra were chosen for chocolate powder due to its higher complexity. Hence, during the MCR-ALS analysis of the mixture samples, three components were used.

Concentration and spectral profiles obtained by the application of the bilinear model of Eq. (2) may not be the correct ones due to the existence of rotational ambiguities (de Juan, Jaumot, & Tauler, 2014b). The bilinear model of Eq. (2) allows that several sets of concentration profiles and spectra with different shapes can reproduce the data **D** with the same precision (de Juan et al., 2014b). In other words, the optimization problem is under-constrained which leads to a great deal of possible solutions. To drive the iterative analysis towards the purest solution, some known information from the system of study can be used as constraints. Examples of constraints include non-negativity and selectivity constraints. The non-negativity constraint can be applied when the resolved spectral data must be positive. The selectivity constraint is used to fix some values in the **S** or **C** matrices. Finally, the spectral profiles can also be normalized to reduce the intensity ambiguity of the solutions (Lawton & Sylvestre, 1971). This ambiguity is caused by the fact that the intensity of spectra can be reproduced by multiple dyads of profiles and concentration with different arbitrary scales (de Juan et al., 2014a).

2.5.1. Augmented matrix

The MCR-ALS algorithm can be used to analyze several samples simultaneously. In fact, by analyzing more than one sample at once, more information relative to the pure components is introduced in the analysis and the possible ambiguities can be substantially reduced. In this work, MCR-ALS was applied to the column-wise augmented data matrix resulting from stacking the 15 unfolded hyperspectral image samples, **X**. This matrix has 55,815 rows and 248 columns (Fig. 2).

2.5.2. Selectivity constraint in the concentration matrix

As stated in section 2.5, an additional constraint can be applied to introduce known information in the MCR-ALS analysis and reduce the ambiguity of the final solution. In the case of the MCR-ALS multiset analysis, the correspondence among constituents and MCR-ALS components allows the introduction of information about the presence or the absence of these constituents in the pixels. In the situation depicted in section 2.1, the composition of the pixels of the pure samples is known, while the composition of every pixel in the mixed powder image is not and therefore it could not be inferred. The correspondence among species, i.e. the selectivity constraint in the **C** matrix (abbreviated as "CSEL") was implemented to constrain only the pure sample images.

With this constraint, components representative of chocolate powder (components 1 and 2) were imposed to not show contribution in pure peanut pixels. Analogously, the component representative of peanut flour (component 3) was imposed to not show contribution in chocolate powder pixels.

In this study, we tested and compared both MCR-ALS resolution methods with and without a selectivity constraint. For simplicity, in this paper, these methods will be referred to as MCR-ALS and MCR-ALS-CSEL, respectively.

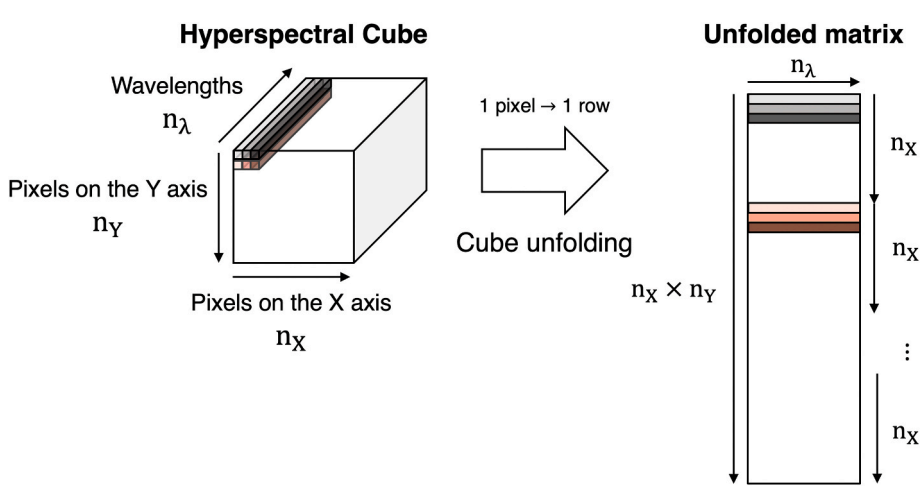

Fig. 1. Hyperspectral cube unfolding. After the unfolding, the hyperspectral cube is transformed into a two-dimensional matrix.

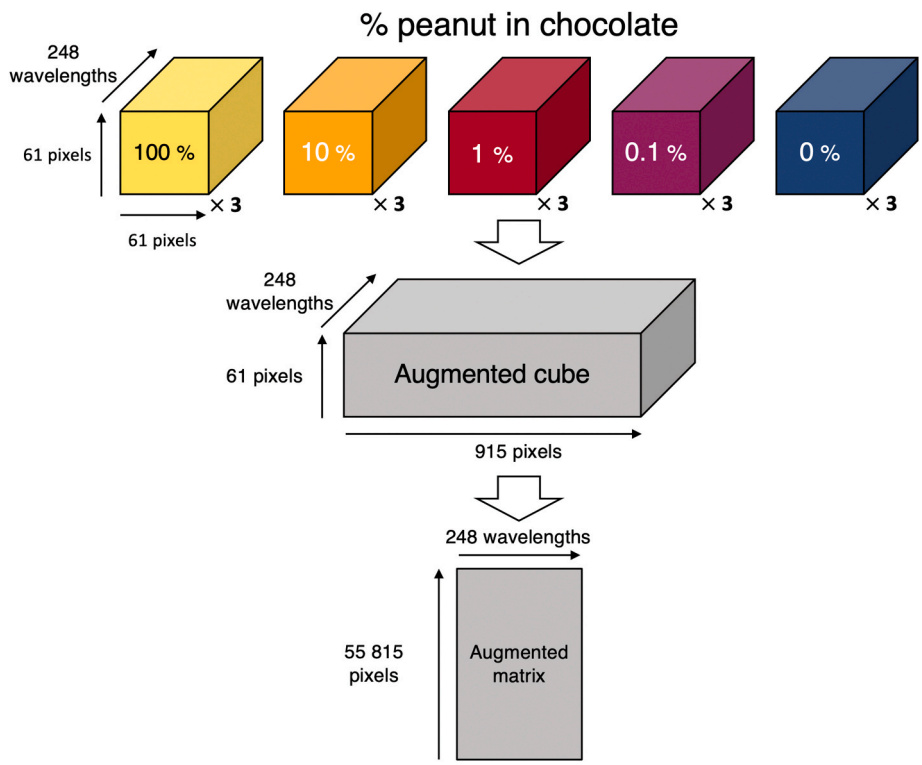

Fig. 2. The hyperspectral cubes (one per sample) are horizontally stacked as an augmented cube, which is unfolded afterwards.

2.6. Detection algorithm

After decomposing the signal of the pixels by MCR-ALS, the resulting **C** matrix was investigated with a detection algorithm to determine the presence or absence of peanut. In this detection algorithm, the **C** matrix was used to build a Gaussian Mixture Model (GMM) (Yang & Ahuja, 1998) on the pure chocolate powder pixels. The GMM consisted of modeling the distribution of points in the 3-dimensional sub-space defined by the 3 MCR-ALS components using several 3D Gaussian distributions. In this study, 2 Gaussians were fitted using the Expectation-Maximization (EM) algorithm (Yang & Ahuja, 1998) to model the distribution of chocolate powder pixels. The Mahalanobis distances between each pixel (represented each with the 3 concentration profiles from the **C** matrix) and both Gaussians were then computed to obtain the score for detection. The threshold for detection was chosen as the highest Mahalanobis distance measured between the GMM and a pixel from the pure chocolate powder samples.

2.7. Software

Data processing were performed in Matlab R2016a (MathWorks Inc.) using the SAISIR toolbox (Cordella & Bertrand, 2014). Processed samples were analyzed with the MCR-ALS method using the MCR-ALS GUI 2.0 under Matlab environment (Jaumot, de Juan, & Tauler, 2015).

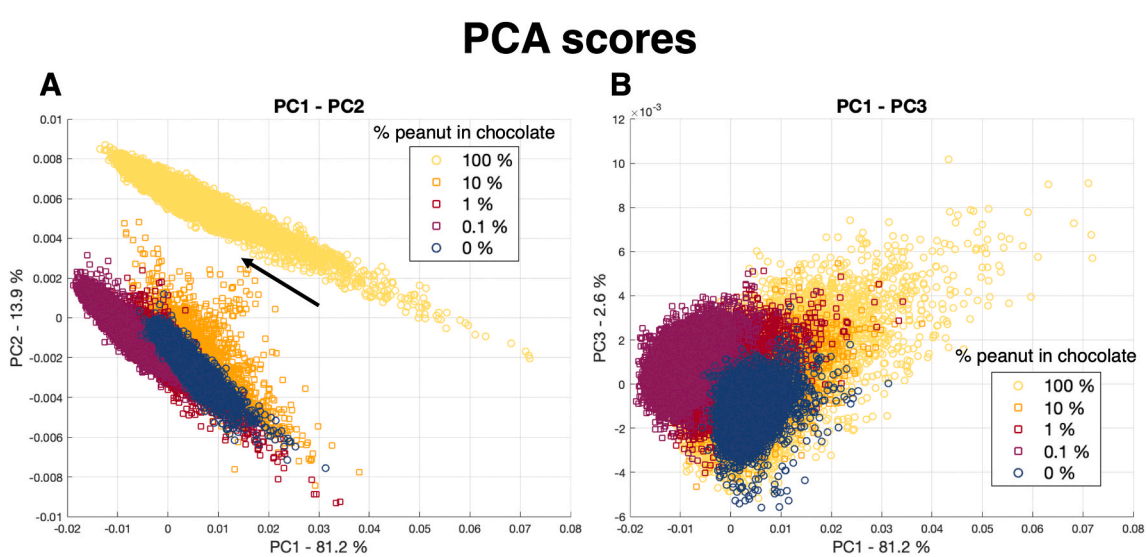

Fig. 3. PCA score plots. The left graph (A) shows the projection of all the pixels on the two first principal components. The black arrow points to the pixels from mixture samples that lie between the chocolate powder and the peanut flour variabilities. The right graph (B) shows the projection of all the pixels on the first and the third principal components.

3. Results and discussion

3.1. Principal Component Analysis

A PCA was first applied to the **X** augmented matrix containing the hyperspectral data from the pixels of all the sample images. The PCA score plot on the first two PCs is given in Fig. 3. In this figure, the scores from the pure peanut flour pixels are clearly separated from those from the pure chocolate powder pixels. Regarding the scores from the mixture samples, they were found clustered around the distribution of pure chocolate pixels scores.

PC1 (81.2% of the total explained variance of the dataset) mainly describes the variability among pixels within the same sample type, while PC2 (13.9% of the explained variance) allows the discrimination of the pure chocolate pixels cluster from the pure peanut pixel cluster. PC3 (2.6% of the explained variance) does not show any separation of the pixels between the pure peanut and the pure chocolate. The same observations were made on the following principal components (results not shown).

The results from this PCA illustrate the so-called "subpixel detection problem" (Bioucas-Dias et al., 2012), since the scores distribution shows that no pixel from the mixture samples is of "pure peanut" as they do not fall into the area of the pure peanut cluster. However, a few scores from the mixture pixels were found between the pure chocolate and the pure

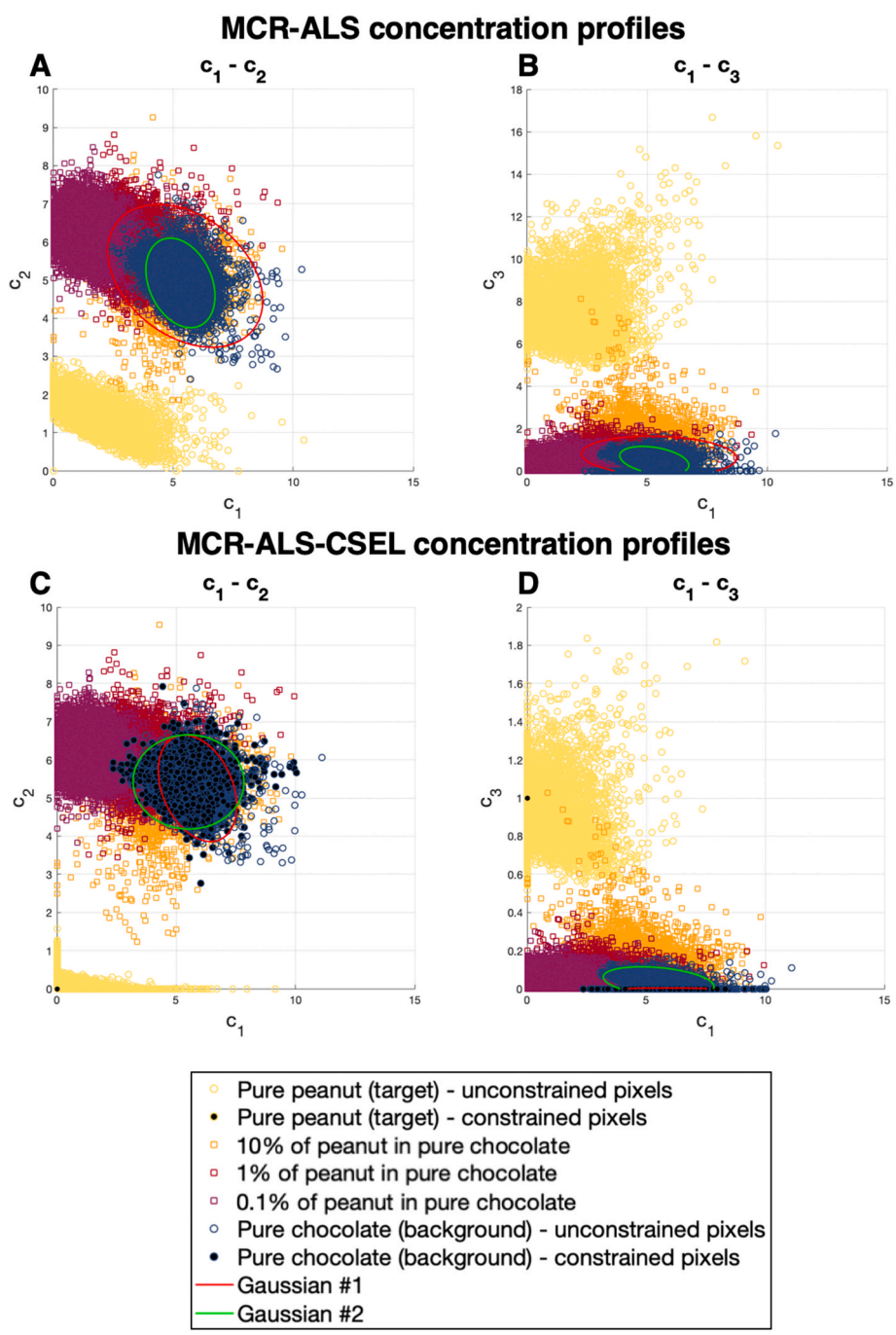

Fig. 4. Scatter plots of the resolved MCR-ALS C concentration profiles. The four subplots show the concentration profiles of each pixel of the dataset for the two methods. (A) and (B) show the results for the MCR-ALS method. (C) and (D) show the results for the MCR-ALS-CSEL method. The ellipses represent the 99% confidence boundaries from the GMM used for the detection method.

peanut variability distributions (see the black arrow in Fig. 3A). These scores represent the pixels from the mixture samples containing, in addition to the spectral signatures from chocolate, the most important spectral contribution from peanut. Nevertheless, these intermediate scores were not observed for pixels from samples containing 1% of peanut, proving that PCA cannot detect peanut adulteration at this concentration level. Therefore, PCA is not an optimal tool to detect peanut pixels in chocolate matrices. We can argue that PCA limitation is derived from the fact that spectral differences linked to the adulteration do not dominate the dataset, since these spectral differences are very small and only occur in a small fraction of the total number of pixels. PCA also imposes the components to be orthogonal to each other. However, this constraint is not representative of the real chemical signatures. Hence, the principal components calculated by PCA do not reflect the true chemical signatures of the mixture problem (de Juan et al., 2014a).

3.2. MCR-ALS

Since PCA could not extract the spectral components in the pixels relative to peanut flour and chocolate powder, MCR-ALS method was applied instead. Fig. 4 shows the **C** concentration profiles for the three MCR-ALS resolved components, which are representative of the pixels. Thus, MCR-ALS results shown in Fig. 4 can be directly compared to the PCA scores shown in Fig. 3. For instance, in Fig. 4, the pure pixels from peanut and chocolate can be discriminated using the third component (c_3) only. On the other hand, two principal components were needed to discriminate the pure samples on the PCA score plot (Fig. 3), demonstrating that MCR-ALS components are much more easily interpretable than the PCA components. The better outcome found for MCR-ALS is mainly derived from the use of the non-negativity constraint that reduced the ambiguity of the data decomposition. Since negative concentrations were not allowed in the resolution of the MCR-ALS model, the spectral components could not compensate for each other. As a result, the spectral shapes of the MCR-ALS components were closer to the pure chemical compounds (Fig. 5).

Consequently, some pixels from the samples containing 10% peanut were found within the pure peanut variability whereas this was not observed in the PCA, which illustrates that MCR-ALS provided a more suitable model for the detection problem of peanut in chocolate powder than the PCA.

Fig. 5 shows the resolved MCR-ALS spectral profiles in blue compared to their initial estimates in black.

The first spectral profile (s_1, Fig. 5A) is descriptive of cocoa as it includes some spectral features characteristics from this constituent as reported elsewhere: the low intensity and spread absorption peak at 1208 nm is due to the combination of the second overtone of CH, CH_2, and CH_3; a higher intensity level absorption can be observed at 1491 nm corresponding to the N–H group characteristic of the proteins in cocoa (Krähmer et al., 2015); the absorption at 1935 nm is attributed to the second overtone of amide C═O (Workman Jr. & Weyer, 2012) which is also descriptive of proteins in cocoa.

The second spectral profile (s_2, Fig. 5B) is descriptive of the sucrose content present in the chocolate powder. The intense absorption peaks at 1435 nm and 2072 nm in s_2 are associated with the C–H stretching and the combination of O–H stretching in sucrose, respectively (da Costa Filho, 2009). Additionally, a double peak at 2280 nm was attributed to the C–H stretching and CH_2 deformation of polysaccharides (Workman Jr. & Weyer, 2012).

The third component is associated with the peanut spectral signature. The peaks at 1474 nm and 1735 nm are related to the N–H second overtone from proteins and to C–H group of amine polysaccharides

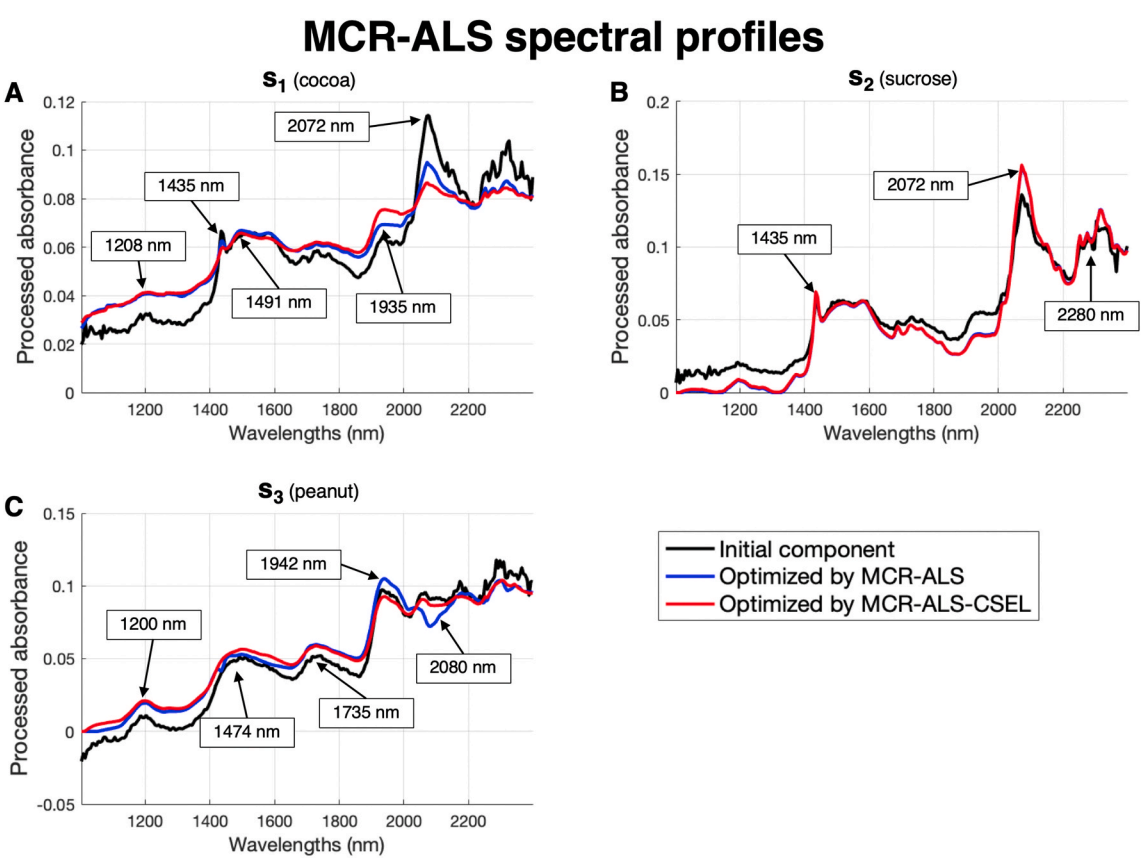

Fig. 5. MCR-ALS optimization of the spectral profiles. The three subplots show the three MCR-ALS components. For each plot, the initial estimate of the component is depicted in black. The resulting spectral profiles obtained by MCR-ALS are given in blue, while the corresponding profiles obtained by MCR-ALS-CSEL are given in red. (For interpretation of the references to color in this figure legend, the reader is referred to the Web version of this article.)

respectively (Workman Jr. & Weyer, 2012). The two main absorption peaks at 1200 nm and 1942 nm are representative of the water absorption contained in the flour. Since the peanuts were defatted before being milled into flour, the fatty acids of peanut were not present in the final product. As a consequence, the near-infrared spectrum of peanut was mainly characterized by its proteins, causing the detection problem to become more difficult as there were fewer spectral signatures characteristic of peanut to be detected in the mixture samples.

Differences between the initial estimates and the final resolved MCR-ALS spectral profiles varied across components. On the one hand, s_2 and s_3 did not change significantly after the MCR-ALS iterative process. This occurred because the pixels chosen as initial estimates were mainly constitutive of the compounds they describe (sucrose and peanut flour, respectively). However, s_1 showed a more prominent alteration of the spectral profile after the iterative process is performed, allegedly because all pixels from cocoa samples contain sucrose and therefore an initial estimate from cocoa without sucrose could not be used. Nevertheless, even without the proper initial estimate for s_1, MCR-ALS reached a satisfactory resolution after the iterative process. This result highlights that the MCR-ALS method is robust enough to extract the pure spectral components of chocolate powder.

The coefficient of correlation between s_1 and s_3 is high ($r^2 = 0.96$), indicating that these spectral profiles of cocoa (without sucrose) and peanut flour are very similar in spectral shape. As a consequence, the obtained MCR-ALS solutions may not be the purest ones due to ambiguities between the two spectra. In fact, this ambiguity could explain why some coefficients c_1 for the pure peanut pixels were not null (Fig. 4). For this reason, the **C** concentration profiles must be read with caution and therefore they should not be used directly for detection purposes.

3.3. MCR-ALS-CSEL

After noticing some spectral ambiguities in the MCR-ALS model performed in the previous section, the MCR-ALS analysis was repeated using CSEL as an additional constraint (see Methods). With CSEL, the value of the **C** concentration profiles can be imposed for certain known pixels, resulting in a reduction of the ambiguity of the system of study. In this work, we imposed that pure peanut pixels only contain spectral signatures from s_3, while pure cocoa pixels only contain spectral signatures from s_1 and s_2.

Table 1 shows the fitting performances of MCR-ALS and MCR-ALS-CSEL. Both methods exhibit high performances with $R^2 > 0.99$. The addition of constraint to the MCR-ALS algorithm leads to consider a tradeoff between the fitting of the data matrix D and the satisfaction of the constraints. Table 1 shows that despite the addition of constraints in the MCR-ALS-CSEL method, the fitting performances are still similar to the MCR-ALS. This indicates that the optimal solution was reached regardless the MCR-ALS method was more constrained. The effect of CSEL can be observed in Fig. 5. In this figure, the spectral profiles resolved with MCR-ALS-CSEL are shown in red, while those resolved with MCR-ALS are shown in blue. Interestingly, some spectral differences can be observed for s_1 and s_3 spectral profiles. On the other hand, s_2 spectral profile remains exactly the same for both methods indicating that the pure profile for this component can be achieved without using the given constraint.

When looking at the differences among the resolved spectral profiles, it can be observed that s_1 and s_3 profiles both differ on similar wavelengths around 2080 nm and 1940 nm. These two spectral patterns are associated with the second overtone of amide group and to the combination O–H stretching, and they can be attributed to both cocoa or peanut constituents. Regarding the unconstrained MCR-ALS method, it resulted in a higher absorption peak at 2072 nm and a smaller absorption peak at 1935 nm in s_1, and a smaller absorption at 2072 nm and a higher absorption at 1935 nm in s_3.

Table 1
The performance in lack of fit and coefficient of determination (R^2) for MCR-ALS and MCR-ALS-CSEL.

	MCR-ALS	MCR-ALS-CSEL
Lack of fit (%)	3.16%	3.27%
R^2	0.9990	0.9989

The CSEL constraint had visible effects on the distribution of pixels in the MCR space (Fig. 4). Fig. 4A and C show the evolution of the distributions for the c_1 and c_2 contributions with and without the application of the CSEL constraint. The main effect observed was the shrinkage of the peanut pixel distribution, which means the variability of the **C** concentration profiles from peanut pixels was reduced after the application of the constraint. The small variability of pure peanut pixels was expected because they do not contain any sucrose nor cocoa and thus the resolved c_1 and c_3 concentrations should be very low.

Fig. 4C and D also showed that, in overall, the distribution of the mixture pixels was not changed by the application of the constraint. Consequently, some scores from mixture pixels were closer to the cluster of peanut distribution for the MCR-ALS-CSEL method. On the other hand, Fig. 4C shows that the cluster of constrained pixels from the chocolate powder pixels is very similar to the cluster of unconstrained pixels showing that the MCR-ALS-CSEL is robust.

These results showed the MCR-ALS-CSEL method was more suitable for solving the unmixing problem than the unconstrained one since it provided concentration profiles more suitable for detection purposes.

3.4. The detection results

In the previous sections, two MCR- ALS methods were used to decompose the spectral signatures found in every pixel into different components representative of the pure sample constituents. In these analyses, two of the resolved components (s_1 and s_2) were representative of chocolate powder while the other (s_3) was of peanut. However, we observed that, for the two MCR-ALS analyses, some pixels from pure (chocolate powder and peanut) samples were decomposed as a mixture of non-zero contributions when at least one of the contributions should have been of 0. The fact that some pure peanut pixels presented $c_1 \neq 0$ and $c_2 \neq 0$ and some chocolate powder pixels presented $c_3 \neq 0$ denote that there was still some ambiguity in the MCR-ALS resolution. This phenomenon also occurred for the non-constrained pure pixels when the MCR-ALS-CSEL method was used, although the abovementioned coefficient contributions were closer to 0 than when the resolution was performed with MCR-ALS. This result suggests that the value given of 0 in c_3 (the component representing peanut) must not be used directly as the threshold level to determine the presence or absence in our samples.

Alternatively, using the lowest value found in c_3 of pure peanut pixels as the threshold level would cause that the detection algorithm is very restrictive (Fig. 4B–D shows that only a few pixels from the 10% adulterated sample would be selected). Instead, a more sophisticated approach is needed to determine peanut adulteration at the pixel level from these MCR-ALS results. For instance, to reduce to a larger extent the ambiguity of the system, it would have been desirable to constrain some pixels from the mixture samples with the CSEL constraint. However, this is unfeasible as the spatial location of the adulterated pixels is not known after performing the mixing.

To overcome this limitation, we implemented a strategy to determine whether a mixture pixel is within the pure chocolate powder variability or not. In the latter situation, the pixel could be considered adulterated. Therefore, to use this method, the only information needed is the product (chocolate powder) variability.

The distribution of pure chocolate pixels in the MCR space was modeled with two Gaussian models using the Expectation-Maximization algorithm (see methods). Two Gaussian models were needed to account for the specific variabilities of the two major ingredients found in chocolate (sucrose and cocoa). The resulting Gaussian models are

represented by the projection of their 99% confidence ellipses in the MCR space in Fig. 4. Important observations can be made from the analysis of the shape of these ellipses. First, the variability of the chocolate powder was effectively reduced on $c_3$when using the CSEL method since the ellipses areas from the **C** concentration profiles obtained in this method were smaller than when the non-constrained method was used. Second, there were a significant amount of mixture pixels with lower c_1 concentration profile than in the pure chocolate powder pixels. Similarly, some other mixture pixels have higher c_3 concentration profile than in the pure chocolate powder pixels. A low c_1 coefficient cannot be regarded as a robust proof of peanut adulteration, as it only indicates that a pixel does not contain a standard amount of cocoa. Conversely, a high c_3 coefficient is undoubtedly indicative of peanut since the associated spectral profile is from this ingredient (Fig. 5). However, since the interpretation of c_1 and c_2 concentration profiles may be required for cases when peanut adulteration is very low, we implemented a detection algorithm that used the information relative to these three concentration profiles.

Specifically, to account for **C** concentration profiles variability, the designed algorithm establishes the peanut adulteration in every pixel on the basis to their Mahalanobis distance with the GMM.

Fig. 6 shows the histograms of the Mahalanobis distances calculated between every pixel and the Mixture of Gaussians from chocolate distribution obtained under both MCR-ALS methods. From this histogram representation, a threshold value that discriminates pure chocolate powder pixels (blue distribution in Fig. 6) from the rest can be estimated. This threshold value corresponds to the highest Mahalanobis distance found for the pure chocolate pixels. Thus, any pixel surpassing this threshold was considered to be adulterated.

Fig. 6 revealed important differences between the distributions obtained from the two MCR-ALS analyses. For instance, the distribution of the Mahalanobis distances for chocolate pixels was narrower when using the CSEL constraint. As a consequence, the detection threshold could be set smaller leading to more positive detection pixels in the mixture samples. This additional detection power derived from the use of the CSEL constraint can be appreciated by comparing the two highlighted regions in Fig. 6. In these regions, it can be observed that a higher number of mixture pixels were considered to be adulterated when the constraint was used.

To assess the reliability of the detection algorithm, the numbers of positive peanut adulteration pixel detections for each sample image were calculated (Table 2). From these numbers, it is observed that all the pure pixels were correctly assigned to chocolate powder or peanut flour. Therefore, the sensitivity and the specificity (calculated from the pure samples) are of 1 for the two methods. This shows that the two methods are reliable to confirm the purity of the samples. Regarding the mixture samples, it is not possible to confirm the validity of the assignment since the actual position of the adulterated pixels in the mixture cannot be known. However, by comparing the proportion of detected adulterated pixels found with the corresponding peanut concentrations, we still can evaluate the quality of the detection algorithm.

Table 2 shows that the number of detections was in line with the global adulteration level. For the mixture samples containing 10% peanut, the MCR-ALS-CSEL method detected between 8.73% and 17.00% of adulterated pixels. On the other hand, for the mixture samples containing 1% peanut, between 0.64% and 1.12% of the pixels were found to be adulterated. The unconstrained MCR-ALS method also found adulterated pixels at these two concentration levels. Nevertheless, the number of positive detections for the unconstrained MCR-ALS method was inferior. The coefficient of correlation was used by Vermeulen et al. to measure the relevancy of the detection rate between adulterated samples (Vermeulen, Ebene, Orlando, Fernández Pierna, & Baeten, 2017). After considering only the adulterated samples, the coefficients of correlation were 0.92 and 0.93 for the detection methods using the MCR-ALS and the MCR-ALS-CSEL respectively.

Regarding the mixture samples with 0.1% adulteration, a few adulterated pixels were found when data were analyzed with the detection algorithm based on the MCR-ALS-CSEL method. However, the same samples were considered to be pure chocolate powder samples when analyzed with the detection algorithm based on the unconstrained MCR-

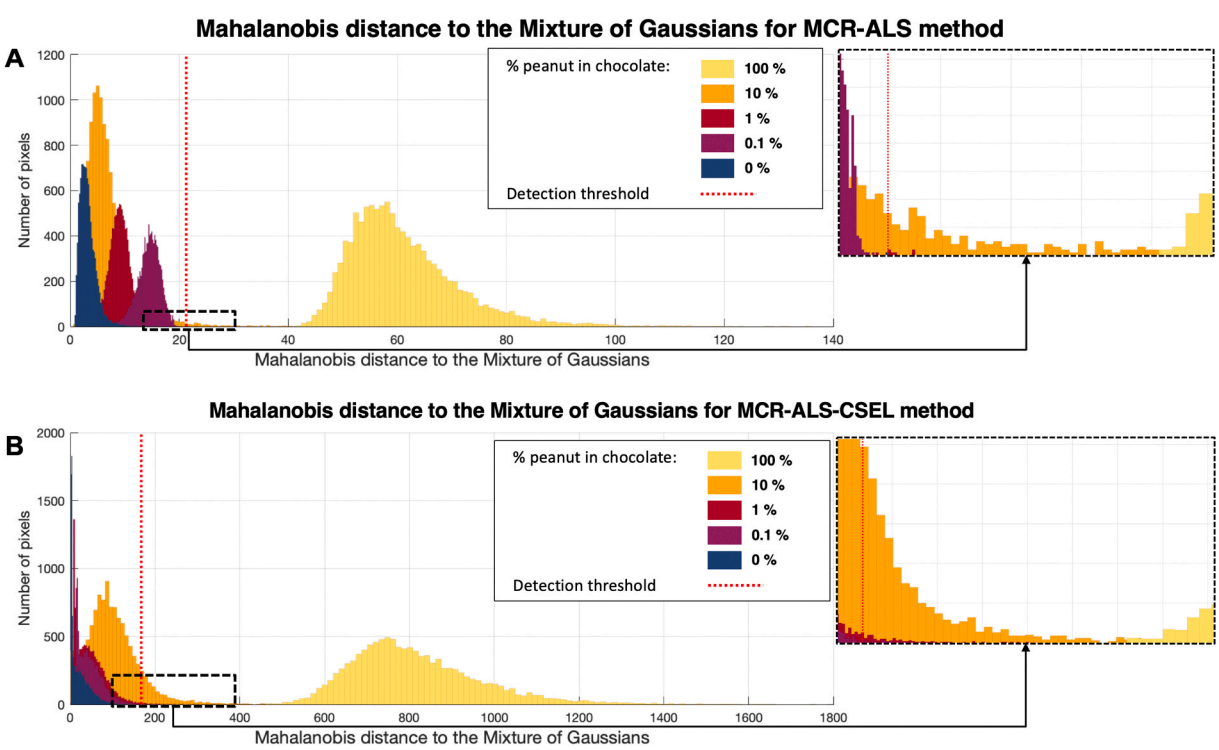

Fig. 6. Histograms of the Mahalanobis distance of every pixel to the GMM. (A) shows the results using the **C** concentration profiles from the unconstrained MCR-ALS method. (B) shows the results using the **C** concentration profiles from the MCR-ALS-CSEL method.

Table 2
Number of detected pixels in each sample image when using the MCR-ALS and the MCR-ALS-CSEL methods. A, B, and C stand for the different sample replicates at each concentration.

Concentration of peanut (%) - replicate	MCR-ALS-CSEL		MCR-ALS	
	Number of detections [a]	Percentage of detection (%) [b]	Number of detections [a]	Percentage of detection (%) [b]
100% - A	3721	100	3721	100
100% - B	3721	100	3721	100
100% - C	3721	100	3721	100
10% - A	382	10.30	45	1.21
10% - B	325	8.73	39	1.05
10% - C	633	17.00	82	2.20
1% - A	29	0.78	2	0.05
1% - B	24	0.64	2	0.05
1% - C	44	1.12	1	0.03
0.1% - A	9	0.24	0	0
0.1% - B	11	0.30	0	0
0.1% - C	1	0.03	0	0
0% - A	0	0	0	0
0% - B	0	0	0	0
0% - B	0	0	0	0

[a] Number of detected pixels in the image containing a total of 3721 pixels.
[b] Proportion of detected pixels with respect to the total number of pixels in the image (3721 pixels).

ALS method. Hence, the algorithm based on MCR-ALS-CSEL has a lower limit of detection than the algorithm based on the unconstrained MCR-ALS.

Fig. 7 shows the spatial positions of the adulterated pixels on the mixture sample image according to both methods. In this figure, it is observed that the adulterated pixels are aggregated in clusters, and these clusters are larger proportionally with the adulteration level. The presence of these clusters, rather than a random distribution of the adulterated pixels, suggests that peanut flour cannot be homogenized easily in the chocolate powder.

Fig. 8 shows the repartition of the particle size of peanut flour and chocolate powder. For peanut, two main modes were observed at 250 μm and 600 μm and the maximal particle size reached 1 mm. However, this particle size distribution did not correspond to the expected particle size of the product. For example, the FAO standard for wheat flour limits the particle size to be less than 212 μm for at least 98% of the particles (Joint FAO/WHO Codex Alimentarius Commission, 1995). The apparition of bigger particle clusters could be explained by the agglomeration phenomena of small particles, which might have occurred during the mixing process. Therefore, the observed clusters of detected pixels in the spectral data correspond to agglomerated peanut particles.

To conclude, the detection maps in Fig. 7 compare both detection methods. These figures, apart from revealing that the MCR-ALS-CSEL method detected much more adulterated pixels than without the constraint, also show that the coincident adulterated pixels were found

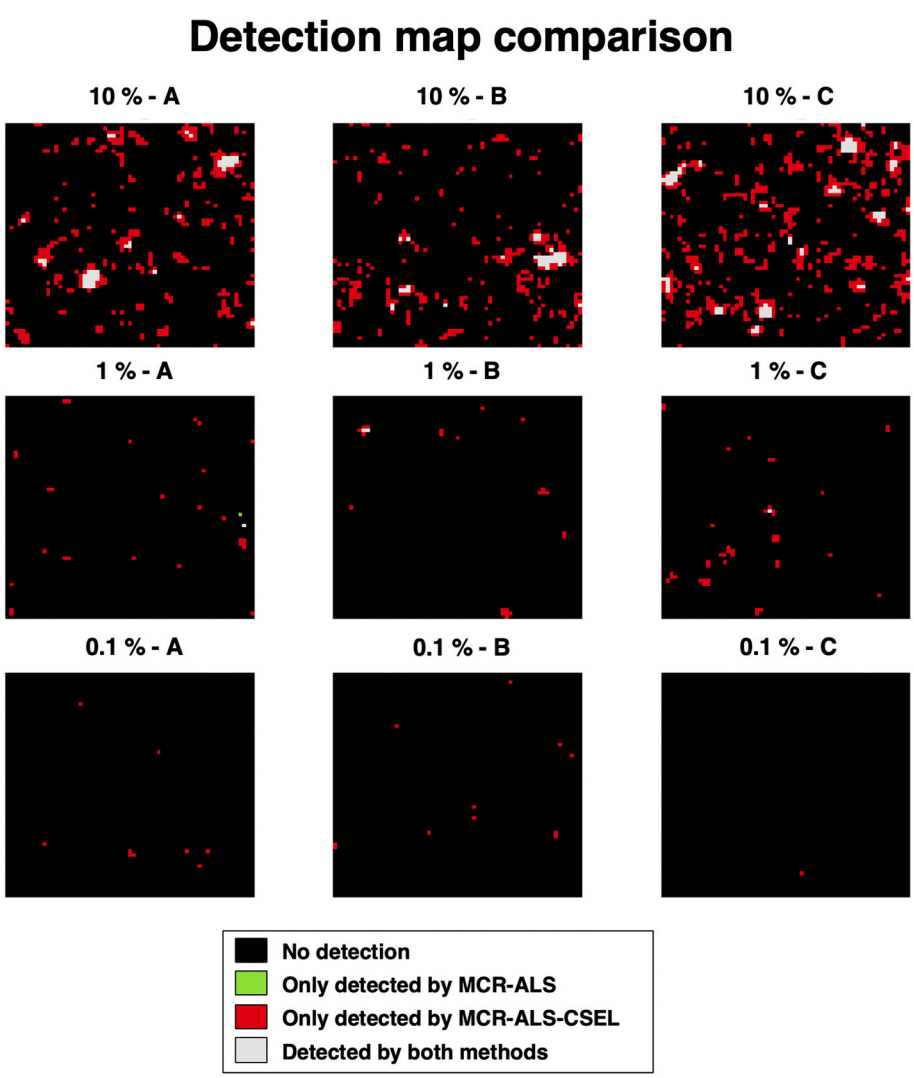

Fig. 7. Each image summarizes the detection map for one sample and the two detection methods: MCR-ALS and MCR-ALS-CSEL. The color code of each pixel indicates the method(s) used showing positive detection. Letters A, B, and C stand for the different replicate samples. These figures are obtained by refolding the C matrix from the MCR-ALS methods and after applying the detection method. (For interpretation of the references to color in this figure legend, the reader is referred to the Web version of this article.)

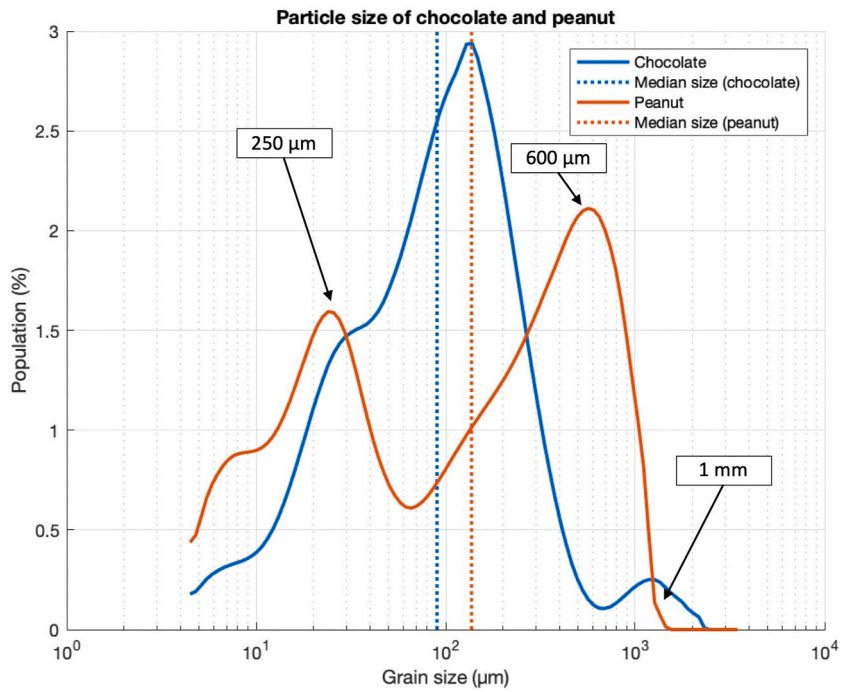

Fig. 8. The particle size distribution of chocolate powder and peanut flour. Data measured with a laser granulometer.

in the center of the clusters. This particular pixel distribution can be explained because those pixels contain a higher quantity of peanut, and therefore are more likely to be recognized by the detection methods as adulterated pixels than those from the outer regions of the clusters.

These results showed that the proposed methods, and in particular the one using MCR-ALS in combination with the CSEL constraint, are very reliable to detect food adulterations even at low concentration levels. The analysis of the adulterated pixels highlighted that the method presented a promising detection power, as the number of adulterated pixels was coincident with the experimental conditions in the terms of signal-response. Moreover, this detection method also revealed that peanut adulteration in chocolate powder is not homogeneous and forms clusters of particles. Despite the spectral similarities of chocolate powder and peanut flour, the presented approach could lead to satisfactory detections of the adulterated pixels. Therefore, this methodology has potential to be used for solving other complex food adulteration systems. Additionally, the detection results showed that low adulteration levels can be detected by screening a small number of pixels. In our case, we were able to detect peanut adulteration in a chocolate powder matrix mixed with 0.1% peanut by only screening 61 × 61 pixels.

4. Conclusion

The capability of near-infrared hyperspectral imaging supported with the chemometric method MCR-ALS to detect peanut flour in chocolate powder was demonstrated.

Detection of adulterated chocolate powder pixels with peanut flour could not be achieved with PCA due to the intrinsic complexity of the problem, as the spectra of chocolate powder and peanut flour are very similar and peanut adulteration occurred at the subpixel level. To cope with this situation, MCR-ALS was used instead. Specifically, we tested two different MCR-ALS methods: a method that incorporates a selectivity constraint and another that does not. The best results were obtained for the constrained MCR-ALS, highlighting that the detection of peanut adulteration in chocolate powder is a very challenging problem.

MCR-ALS results were used to build a metric for assessing peanut adulteration. With this metric, we were able to detect peanut adulteration in all the contaminated samples. On the other hand, a selectivity and sensitivity of 1 were obtained on the pure samples. A correlation of 0.92 and 0.93 were obtained between the number of adulterated pixels and the real concentration of mixed samples for MCR-ALS and MCR-ALS-CSEL respectively. These results support the fact that the selectivity constraint was efficient to obtain spectral profiles closer to the real ones and to detect more adulterated pixels.

Due to its high performance, the method has the potential to be used for similar systems involving powder samples. Future work will be carried out to optimize the data acquisition and measurement, accounting by the sensitivity of the hyperspectral camera and the penetration depth of the near-infrared radiations. More advanced technique could also be used to optimize the MCR-ALS algorithm locally. For instance, the local rank analysis enables to estimate the complexity of a neighborhood of pixels to set the number of component (De Juan, Maeder, Hancewicz, & Tauler, 2005). Using this method, the MCR-ALS fitting may be improved locally.

Funding

This work was funded by the Infrastructure Biologie Santé “Phenome FPPN” supported by the National Research Agency and the “Programme d’Investissements d’Avenir” (PIA) (ANR-11-INBS0012).

Declaration of competing interest

The authors declare that they have no known competing financial interests or personal relationships that could have appeared to influence the work reported in this paper.

CRediT authorship contribution statement

Antoine Laborde: Conceptualization, Methodology, Formal analysis, Writing - original draft, Visualization, Investigation. **Francesc Puig-Castellví:** Conceptualization, Methodology, Formal analysis, Writing - review & editing, Visualization, Validation. **Delphine Jouan-Rimbaud Bouveresse:** Writing - review & editing. **Luc Eveleigh:** Writing - review & editing. **Christophe Cordella:** Writing - review & editing, Supervision, Project administration. **Benoît Jaillais:**

Methodology, Resources, Validation, Writing - review & editing, Supervision, Project administration.

Acknowledgements

We want to thank Joaquim Jaumot and Silvia Mas García for the insightful discussions regarding MCR-ALS and its implementation.

References

Bioucas-Dias, J. M., Plaza, A., Dobigeon, N., Parente, M., Du, Q., Gader, P., et al. (2012). Hyperspectral unmixing overview: Geometrical, statistical, and sparse regression-based approaches. *IEEE J. Selected Topics Appl. Earth Obser.Rem. Sens., 5*(2), 354–379. https://doi.org/10.1109/JSTARS.2012.2194696.

Boiret, M., de Juan, A., Gorretta, N., Ginot, Y. M., & Roger, J. M. (2015). Distribution of a low dose compound within pharmaceutical tablet by using multivariate curve resolution on Raman hyperspectral images. *Journal of Pharmaceutical and Biomedical Analysis, 103*, 35–43. https://doi.org/10.1016/j.jpba.2014.10.024.

Chang, A. S., Sreedharan, A., & Schneider, K. R. (2013). Peanut and peanut products: A food safety perspective. *Food Control, 32*(1), 296–303. https://doi.org/10.1016/j.foodcont.2012.12.007.

Cordella, C. B. Y., & Bertrand, D. (2014). Saisir: A new general chemometric toolbox. *TrAC - Trends in Analytical Chemistry, 54*, 75–82. https://doi.org/10.1016/j.trac.2013.10.009.

da Costa Filho, P. A. (2009). Rapid determination of sucrose in chocolate mass using near infrared spectroscopy. *Analytica Chimica Acta, 631*(2), 206–211. https://doi.org/10.1016/j.aca.2008.10.049.

De Juan, A., Maeder, M., Hancewicz, T., & Tauler, R. (2005). Local rank analysis for exploratory spectroscopic image analysis. Fixed Size Image Window-Evolving Factor Analysis. *Chemometrics and Intelligent Laboratory Systems, 77*, 64–74. https://doi.org/10.1016/j.chemolab.2004.11.006, 1-2 SPEC. ISS.

Fernández Pierna, J. A., Vincke, D., Dardenne, P., Yang, Z., Han, L., & Baeten, V. (2014). Line scan hyperspectral imaging spectroscopyfor the early detection of melamineand cyanuric acid in feed. *Journal of Near Infrared Spectroscopy, 22*(2), 103–112. https://doi.org/10.1255/jnirs.1109.

Fitzpatrick, J. J., & Ahrné, L. (2005). Food powder handling and processing : Industry problems , knowledge barriers and research opportunities. *Chemical Engineering and Processing, 44*, 209–214. https://doi.org/10.1016/j.cep.2004.03.014.

Fu, X., Kim, M. S., Chao, K., Qin, J., Lim, J., Lee, H., et al. (2014). Detection of melamine in milk powders based on NIR hyperspectral imaging and spectral similarity analyses. *Journal of Food Engineering, 124*, 97–104. https://doi.org/10.1016/j.jfoodeng.2013.09.023.

Geladi, P., Burger, J., & Lestander, T. (2004). Hyperspectral imaging : Calibration problems and solutions. *Chemometrics and Intelligent Laboratory Systems, 72*, 209–217. https://doi.org/10.1016/j.chemolab.2004.01.023.

Golub, G. H., & Reinsch, C. (1970). Comparacion de inhibicion de La prueba cutanea de La histamina con astemizole, loratadina Y terfenadina. *Numerische Mathematik, 14*, 403–420.

Gowen, A. A., O'Donnell, C. P., Cullen, P. J., Downey, G., & Frias, J. M. (2007). Hyperspectral imaging - an emerging process analytical tool for food quality and safety control. *Trends in Food Science & Technology, 18*(12), 590–598. https://doi.org/10.1016/j.tifs.2007.06.001.

Hefle, S. L., & Taylor, S. L. (2004). Food allergy and the food industry. *Current Allergy and Asthma Reports, 4*(1), 55–59. https://doi.org/10.1007/s11882-004-0044-y.

van Hengel, A. J. (2007). Food allergen detection methods and the challenge to protect food-allergic consumers. *Analytical and Bioanalytical Chemistry, 389*(1), 111–118. https://doi.org/10.1007/s00216-007-1353-5.

Huang, M., Kim, M. S., Delwiche, S. R., Chao, K., Qin, J., Mo, C., et al. (2016). Quantitative analysis of melamine in milk powders using near-infrared hyperspectral imaging and band ratio. *Journal of Food Engineering, 181*, 10–19. https://doi.org/10.1016/j.jfoodeng.2016.02.017.

Huang, Y., Tian, K., Min, S., Xiong, Y., & Du, G. (2015). Distribution assessment and quantification of counterfeit melamine in powdered milk by NIR imaging methods. *Food Chemistry, 177*, 174–181. https://doi.org/10.1016/j.foodchem.2015.01.029.

INRA, & ANSES. (2015). *Étude des allergènes dans les produits transformés disponibles sur le marché français entre 2008 et 2012*.

Jaumot, J., de Juan, A., & Tauler, R. (2015). MCR-ALS GUI 2.0: New features and applications. *Chemometrics and Intelligent Laboratory Systems, 140*, 1–12. https://doi.org/10.1016/j.chemolab.2014.10.003.

Jin, H., Ma, Y., Li, L., & Cheng, J. H. (2016). Rapid and non-destructive determination of oil content of peanut (Arachis hypogaea L.) using hyperspectral imaging analysis. *Food Anal. Methods, 9*(7), 2060–2067. https://doi.org/10.1007/s12161-015-0384-3.

Joint FAO/WHO Codex Alimentarius Commission. (1995). Codex standard 152–1985 "wheat flour. In *In Codex Alimentarius*.

de Juan, A. (2020). Multivariate curve resolution for hyperspectral image analysis. *Data Handling in Science and Technology, 32*. https://doi.org/10.1016/B978-0-444-63977-6.00007-9.

de Juan, A., Jaumot, J., & Tauler, R. (2014a). Multivariate Curve Resolution (MCR). Solving the mixture analysis problem. *Anal. Methods, 6*(14), 4964–4976. https://doi.org/10.1039/c4ay00571f.

de Juan, A., Jaumot, J., & Tauler, R. (2014b). Multivariate Curve Resolution (MCR). Solving the mixture analysis problem. *Anal. Methods, 6*(14), 4964–4976. https://doi.org/10.1039/c4ay00571f.

Krähmer, Andrea, Engel, Annika, Kadow, Daniel, Ali, Naailah, Umaharan, Pathmanathan, Kroh, Lothar, W, & Schulz, Hartwig (2015). Fast and neat – Determination of biochemical quality parameters in cocoa using near infrared spectroscopy. *Food Chemistry, 181*, 152–159. https://doi.org/10.1016/j.foodchem.2015.02.084.

Laborde, A., Jaillais, B., Bendoula, R., Roger, J., Bouveresse, D. J.-R., Eveleigh, L., et al. (2019). A partial least squares-based approach to assess the light penetration depth in wheat flour by near infrared hyperspectral imaging. *Journal of Near Infrared Spectroscopy, 28*(1), 25–36. https://doi.org/10.1177/0967033519891594.

Lancelot, E., Bertrand, D., Hanafi, M., & Jaillais, B. (2017). Near-Infrared hyperspectral imaging for following imbibition imbibition of single wheat kernel sections. *Vibrational Spectroscopy, 92*, 46–53. https://doi.org/10.1016/j.vibspec.2017.05.001.

Lawton, W. H., & Sylvestre, E. A. (1971). Self modeling curve resolution. *Technometrics, 13*(3), 617–633. https://doi.org/10.1002/0471667196.ess0035.pub2.

Lohumi, S., Lee, S., Lee, H., & Cho, B. K. (2015). A review of vibrational spectroscopic techniques for the detection of food authenticity and adulteration. *Trends in Food Science & Technology, 46*(1), 85–98. https://doi.org/10.1016/j.tifs.2015.08.003.

Mishra, P., Cordella, C. B. Y., Rutledge, D. N., Barreiro, P., Roger, J. M., & Diezma, B. (2016). Application of independent components analysis with the JADE algorithm and NIR hyperspectral imaging for revealing food adulteration. *Journal of Food Engineering, 168*, 7–15. https://doi.org/10.1016/j.jfoodeng.2015.07.008.

Mishra, P., Herrero-Langreo, A., Barreiro, P., & Roger, J. M. (2015). Detection and quantification of peanut traces in wheat flour by near infrared hyperspectral imaging spectroscopy using principal-component analysis. *Journal of Near Infrared Spectroscopy, 23*(1), 15–22. https://doi.org/10.1255/jnirs.1142.

Moneret-Vautrin, D. A., & Kanny, G. (2004). Update on threshold doses of food allergens: Implications for patients and the food industry. *Current Opinion in Allergy and Clinical Immunology, 4*(3), 215–219. https://doi.org/10.1097/00130832-200406000-00014.

Olmos, V., Benítez, L., Marro, M., Loza-Alvarez, P., Piña, B., Tauler, R., et al. (2017). Relevant aspects of unmixing/resolution analysis for the interpretation of biological vibrational hyperspectral images. *TrAC - Trends in Analytical Chemistry, 94*, 130–140. https://doi.org/10.1016/j.trac.2017.07.004.

Tauler, R., & Kowalski, B. R. (1993). MCR applied to spectral data from multiple runs of an industrial process. *Analytical Chemistry, 65*(11), 2040–2047. Retrieved from https://pubs.acs.org/sharingguidelines.

Vermeulen, P., Ebene, M. B., Orlando, B., Fernández Pierna, J. A., & Baeten, V. (2017). Online detection and quantification of particles of ergot bodies in cereal flour using near-infrared hyperspectral imaging. *Food Additives & Contaminants Part A Chemistry, Analysis, Control, Exposure and Risk Assessment, 34*(8), 1312–1319. https://doi.org/10.1080/19440049.2017.1336798.

Workman, J., Jr., & Weyer, L. (2012). *Practical guide and spectral atlas for interpretive near-infrared spectroscopy (CRC press)*. Boca Raton: CRC Press.

Yang, M., & Ahuja, N. (1998). Gaussian mixture model for human skin color and its applications in image and video Databases_Image. In *, Vol. 3656. Proceedings volume 3656, storage and retrieval for image and video databases VII* (pp. 458–466). January.